ISSN (Print) 1226-1750
ISSN (Online) 2233-6656
Journal of Magnetics 28(4), 443-448 (2023) https://doi.org/10.4283/JMAG.2023.28.4.443

Application of Effective Atomic Number for Contrast Agent Imaging using Dual-energy Computed Tomography: A Simulation Study

Kihong Son[1], Seunghyung Lee[2], Hyobin Lee[2], Yejin Lee[2], Dongwook Son[2], Seunghyeon Myeong[2], Minjoo Chang[2], Daehong Kim[2]*, and Myung-Ae Chung[3]*

[1]Medical Information Research Section, Electronic and Telecommunications Research Institute, Deajeon 34129, Republic of Korea
[2]Department of Radiological Science, Eulji University, Seongnam 13135, Republic of Korea
[3]Department of BigData Medical Convergence, Eulji University, Seongnam 13135, Republic of Korea

(Received 18 October 2023, Received in final form 29 November 2023, Accepted 5 December 2023)

This simulation study aims to differentiate between contrast media and calcification in blood vessel using the effective atomic number (EAN) extraction method in electromagnetic X-ray computed tomography (CT) imaging. Calibration was performed on six tissue-equivalent materials, three contrast medium, and one calcium solution. The Hounsfield unit (HU) values at 80 kV and 140 kV with electromagnetic spectrum using dual-energy computed tomography (DECT) facilitated this calibration. EAN from the polynomial method was then compared with that from the Stoichiometric method. In 120 kV vascular imaging, when the HU of calcium and iodine contrast media were alike, EAN provided a more pronounced contrast than HU. The iodine contrast agent's enhancement in EAN was approximately 30.0 %, and in HU, it was 13.0 % relative to calcium. This indicates EAN's potential to better differentiate contrast media from calcification in clinical contexts.

Keywords : electromagnetic X-ray, effective atomic number (EAN), electromagnetic spectrum, polynomial fitting method, dual-energy computed tomography (DECT)

1. Introduction

Computed tomography (CT) is an imaging modality that is well established as a clinical standard for diagnose, attributing to its capability to produce a three-dimensional image of the anatomy with short scan time. CT utilizes a rotating beam of x-ray that undergoes differential attenuation as it travels through anatomical slices of different tissue composition before it reaches the detector and processed as an image. Attenuation of the x-ray is governed by both the electron density of the medium as well as the beam quality, in this case the peak tube potential (kVp). However, differentiating materials that exhibit similar attenuation at a certain energy was a challenge which became one the rationales behind the development of dual-energy CT (DECT). DECT implements two tube energies, one at low kVp and one at high kVp, and is used for spectroscopy, material decomposition, and contrast enhancement [1, 2]. One of the prominent areas of clinical application of DECT is the identification of coronary artery disease (CAD), especially the atherosclerosis where a plaque obstructs the blood flow and leads to serious complications [3]. Depending on the material composition of the plaque, atherosclerosis is further classified into calcified and non-calcified coronary artery plaques. CAD remains to be one of the leading causes of death in the United States [4], therefore the ability to detect and accurately image the intravascular plaque is of importance.

Calcification that exists in small vasculature such as coronary arteries poses a challenge when distinguishing between iodine contrast due to overlapping Hounsfield unit (HU) between them, setting in motion several studies that addressed the problem. Feuerlein *et al.* proposed a methodoloy to distinguish intravasculature calcification from gadolinum contrast using photon-counting detector which involves the implementation of multiple energy bins to enhance the contrast between plaque and gadolinum contrast [5]. Nair *et al.* reports superior visualization of calcified plaque and residual lumen from dual-energy CT angiography's (DECTA's) algorithmic

*Corresponding author: Tel: +82-31-740-7494
Fax: +82-31-740-7351, e-mail: machung@eulji.ac.kr
goldcollar011@eulji.ac.kr

approach [6]. Nakajima *et al.* used DECT to obtain the effective atomic number (EAN) of non-calcified coronary plaques (NCCPs) and compared it with the intravascular untrasonography (IVUS), reporting DECT-derived EAN to better classify NCCPs compared to that of a conventional single-energy CT (SECT) [7].

Subsequent investigations that aimed to identify and quantify the calcification in the artery pursued. However, a parallel effort to quantify the calcification as well as enhancing the contrast against the adjacent contrast material has not yet been made to the best of our knowledge. Hence, the aim of this study is to propose a methodology via simulation to enhance calcification detection and contrast between calcification and contrast material using their respective EAN, extracted from DECT. Simulation was run using various information on tissue equivalent material, contrast material and calcification material. The ratio of the attenuation coefficient obtained from EAN and DECT was calibrated and expressed as an EAN image. Improvement in the fitting accuracy was made using polynomial approach and the result is compared with the well established Stoichiometric calibration method.

2. Materials and Methods

Multiple methods exist regarding the calibration of materials of various EAN and attenuation ratios under high and low energy x-ray. Schneider *et al.* suggested a Stoichiometric calibration that takes into consideration of material's linear attenuation coefficient and therefore includes relevant photon interaction modes such as classical scatter, photoelectric effect and Compton scatter; The Stoichiometric calibration is considered to show higher accuracy among other calibration methods [8]. This study applied a polynomial approximation to the calibration of material's attenuation ratio between high and low energy, with an aim to improve fitting accuracy compared to the established Stoichiometric calibration. Chang *et al.* provides the following equation (1), describing a relationship between a material's EAN and attenuation coefficient that can be fitted by a polynomial regression model [9].

$$\frac{HU_L + 1{,}000}{HU_H + 1{,}000} = \Sigma_{n=0}^{i} a_n (Z_{eff})^n \quad (1)$$

Here, a_n is the i^{th} coefficient term and Z_{eff} is the nomenclature interchangeably used with EAN. Materials used for calibration are six tissue-equivalent materials: adipose, breast, solid water, liver, inner bone, cortical bone. Three iodine contrast solutions of different concentration and a calcium solution was also used. Table 1 reports the EAN and HUs of low energy (80 kV) and high energy (140 kV), respectively, of the materials used for calibration [10]. Fig. 1 shows the phantom image of 10 above mentioned materials, created based on the HU units obtained under 80 and 140 kV tube potentials. In fitting the relationship between EAN and attenuation coefficient, a third-degree polynomial was used which follows the trend line closely with high R^2 and is produced below as equation (2).

$$\frac{HU_L + 1{,}000}{HU_H + 1{,}000} = a \times Z_{eff}^3 + b \times Z_{eff}^2 + c \times Z_{eff} + d \quad (2)$$

Here, a, b, c, and d are the coefficients obtained from fitting the ratio between EAN and attenuation coefficient of 10 materials presented in Table 1 using a third-degree polynomial with a resulting R^2 of 0.9961.

Table 1. Effective atomic number (EAN) information for various materials. HU values were described for calibration and generating phantom [10].

No.	Materials	EAN	HU		
			80 kV	120 kV	140 kV
1	Adipose	6.44	-118.3	-98.6	-95.5
2	Breast	6.90	-60.2	-51.0	-50.9
3	Solid water	7.24	1.4	-4.3	-7.2
4	Liver	7.60	77.1	72.5	70.2
5	Iodine (2 mg/mL)	8.37	80.0	51.0	37.0
6	Calcium (100 mg/mL)	9.87	407.0	325.8	288.0
7	Inner bone	10.01	299.9	207.1	184.6
8	Iodine (10 mg/mL)	11.25	400.0	235.0	194.0
9	Iodine (15 mg/mL)	12.49	562.5	369.0	262.0
10	Cortical bone	13.29	1670.3	1207.9	1103.7

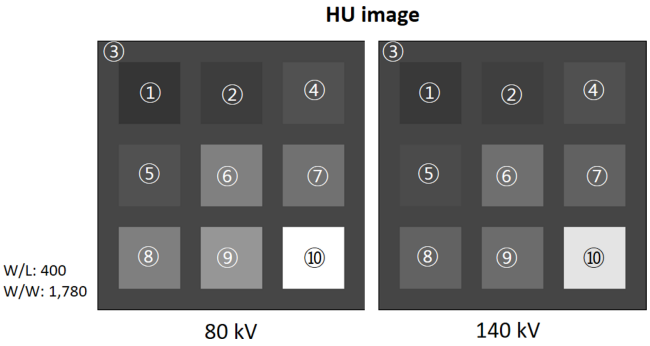

Fig. 1. Low-energy (80 kV) and high-energy (140 kV) phantom images were created with the HU values of the materials in Table 1.

To compare the fitting result obtained using polynomial fitting, Stoichiometric calibration methodology of Schneider *et al.* [11], represented below as an equation (3), was carried out.

$$\frac{HU_L + 1{,}000}{HU_H + 1{,}000} = \frac{1 + k_{1,L} \times z_{eff}^{1.86} + k_{2,L} \times z_{eff}^{3.62}}{1 + k_{1,L} \times z_w^{1.86} + k_{2,L} \times z_w^{3.62}} \times \frac{1 + k_{1,H} \times z_w^{1.86} + k_{2,H} \times z_w^{3.62}}{1 + k_{1,H} \times z_{eff}^{1.86} + k_{2,H} \times z_{eff}^{3.62}} \quad (3)$$

Here, Z_w is the EAN of water and Z_{eff}, the EAN of a material. $K_{1,L}$, $K_{2,L}$, $K_{1,H}$, $K_{2,H}$ are the fitting parameters. Obtained coefficients and fitting parameters from the polynomial approach (eq. (2)) and Stoichiometric methodology (eq. (3)) is tabulated in Table 2.

Similarly with the polynomial approach, calibration data of 10 materials listed in Table 1 is used for fitting with a resulting R^2 of 0.9958. Fig. 2 depicts calibration data, along with calibration curves obtained from two methodologies, polynomial and stoichiometry method and shows superior R^2 of polynomial method against stoichiometry method. Fig. 3 illustrates the residuals of two respective methodologies. Largest residual for Stoichiometric method is reported to be about -0.008 for an inner bone with an EAN of 10. Regarding the largest residual of polynomial method, it is shown to be at the

Table 2. Coefficients and fitting parameters obtained from fitting using polynomial approximation and Stoichiometric method.

Coefficient	Polynomial	Coefficient	Stoichiometric
a	-0.0003	$K_{1,L}$	0.4307
b	0.0115	$K_{2,L}$	0.0030
c	-0.0912	$K_{1,H}$	3.4490
d	1.1720	$K_{2,H}$	-0.0015

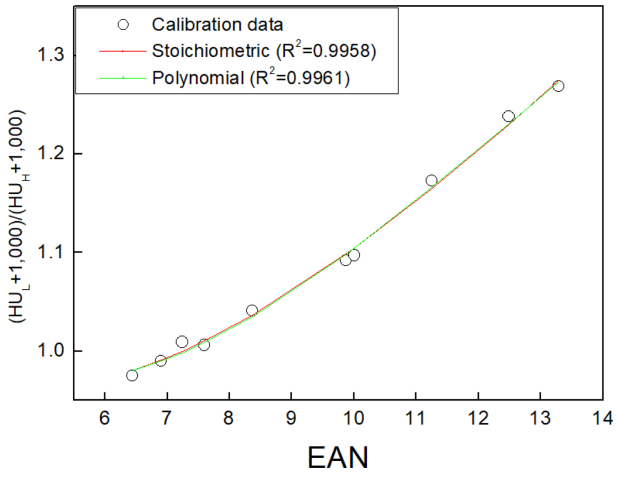

Fig. 2. (Color online) The dots (black) are the ratio of the attenuation coefficients of the materials for calibration, and the solid line (red, light green) is the fitting curve of the dots.

EAN corresponding to a solid water as 0.011. Throughout most materials in polynomial approach showed smaller residual compared to that of Stoichiometric.

3. Results

10 materials listed in Fig. 1 was calibrated using polynomial approach and Stoichiometric method, then an EAN image was obtained with iterative algorithm. Coefficient obtained from polynomial approach was applied to eq. (2), and EAN image was obtained through an iterative process using HU image of 80 kV and 140 kV as shown in Fig. 1. The initial condition of the EAN set within the iteration algorithm was set to 5, considering the lowest EAN number of 6.44 (adipose) used in this

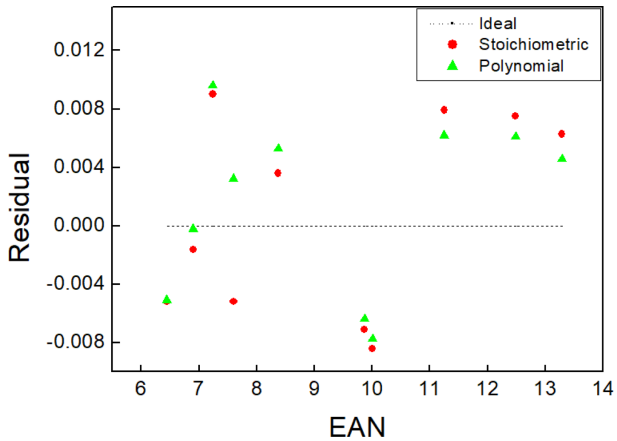

Fig. 3. (Color online) Residuals for all materials were generally smaller in the polynomial approximation than in the Stoichiometric method.

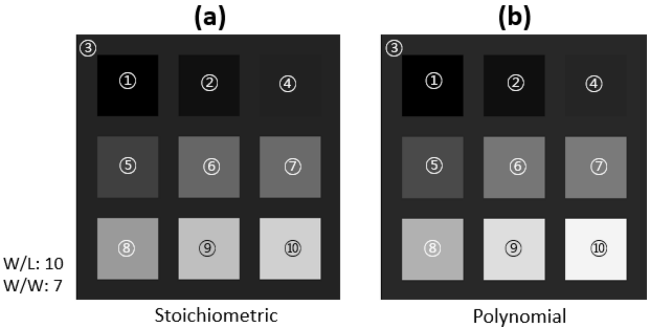

Fig. 4. Effective atomic number (EAN) image based on Stoichiometric (a) and polynomial methods (b) for 10 materials in Table 1.

study. The iteration algorithm is programmed with MATLAB (R2013b, MathWorks Inc, MA, US). Computing environment used in this study include Intel Core i7 2.50 GHz CPU which took 15 minutes in computing the EAN image of the matrix of size 512 × 512. Stoichiometric methodology followed an identical workflow in producing the EAN image.

Figure 4 illustrates the EAN image (W/L: 10, W/W: 7) of the 10 materials obtained through an iterative algorithm, each processed with a polynomial approach and Stoichiometric methodology. Fig. 5 reports the theoretical EANs of the materials compared to the experimental values. Dotted line (black) represents the theoretical EAN, and results obtained by polynomial approach shows closer adherence to the theoretical values compared to that of Stoichiometric method. Fig. 6 re-illustrates the data presented in Fig. 4 as a percentage error from the theoretical value. Mean percent error of the Stoichiometric result reported 3.82 %, with largest

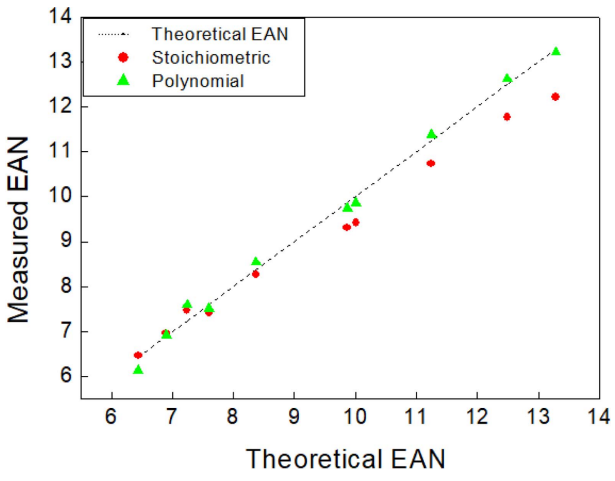

Fig. 5. (Color online) Theoretical and measured EAN for 10 materials. The closer to the dotted line (black), the higher the accuracy of the measured value.

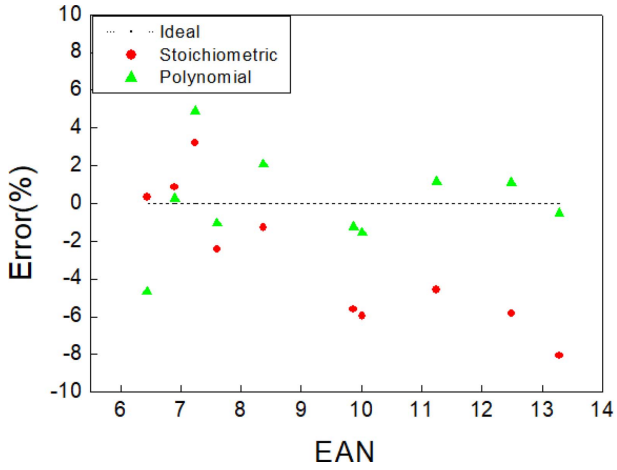

Fig. 6. (Color online) The mean errors of the EAN obtained by the Stoichiometric and polynomial method are 3.82 % and 1.82 %, respectively.

deviance from the theoretical value found in the cortical bone of EAN 13.29 as -8.06 %. In the case of the polynomial approach, mean percent error reported 1.82 % with largest deviance was from the adipose tissue of EAN 6.44 as -4.67 %.

Figure 7 illustrates the scenario of a blood vessel with calcium and contrast present which is challenging for the conventional SECT image to distinguish between. Improvement in contrast was confirmed in an EAN image of the same scenario compared to HU image. The contrast used for simulation corresponding to Fig. 7 is iodine (15 mg/mL), with calcium (100 mg/mL) representing calcification material. The tube energy was set to be 120 kV, a typical tube potential for a conventional CT. HU value of iodine and calcium was taken from the corresponding values depicted in Table 1 as 369.0 and 325.8 HU, respectively.

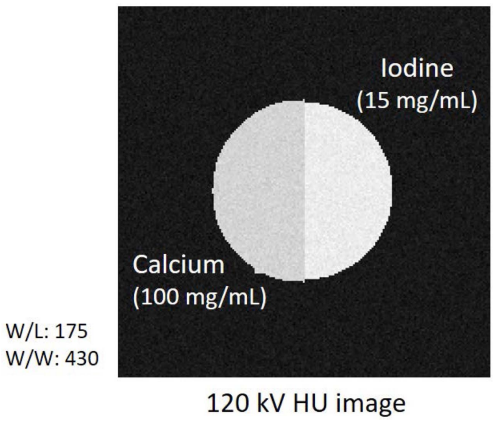

Fig. 7. HU images of calcium (100 mg/mL) and iodine (15 mg/mL) contrast agents acquired at 120 kV.

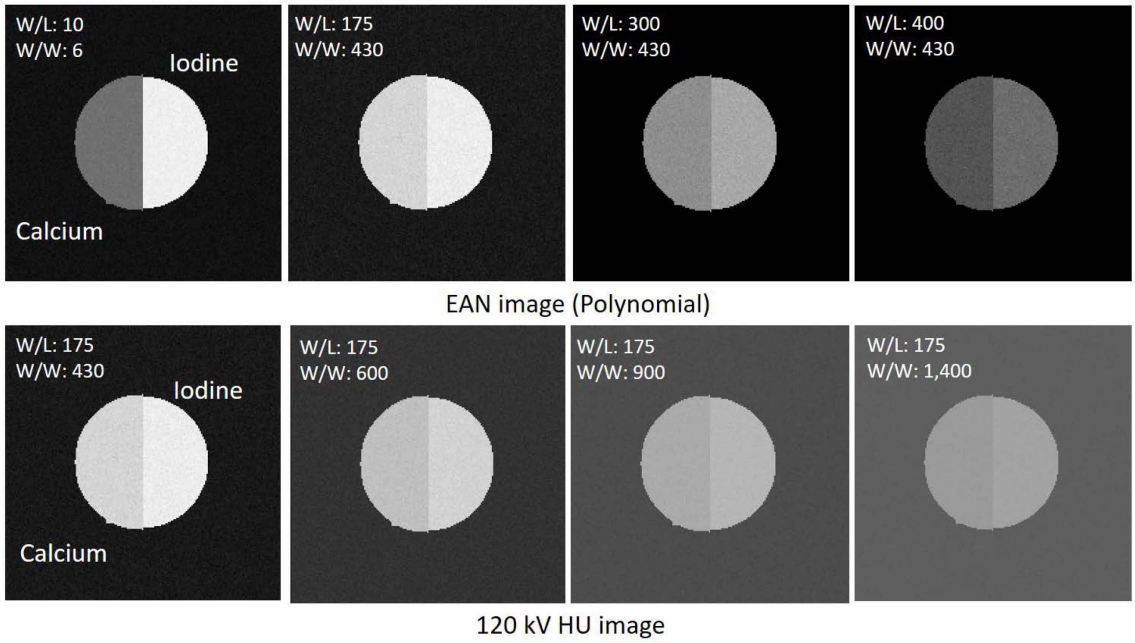

Fig. 8. In the 120 kV HU image and EAN image, iodine (15 mg/mL) showed a contrast increase of 13.0 % and 30.0 %, respectively, compared to calcium (100 mg/mL).

For the same simulation space consisting of contrast and calcification material, EAN image was obtained using polynomial approach. Fig. 8 shows comparison between the said EAN image and HU image. The contrast increase for iodine (15 mg/mL) showed 13.0 % increase in contrast compared to calcium (100 mg/mL) for a 120 kV HU image simulation. Comparatively, for EAN image simulation the contrast increase for iodine showed 30.0 % increase in contrast compared to calcium. Additionally, the effect of various window width and window level was investigated and demonstrated that the HU image showed limited improvement in contrast compared to its EAN image counterparts.

4. Discussion

This study has proposed a methodology of image contrast and differentiation enhancement between previously challenging scenario of adjacent materials of similar HU value (Iodine contrast and calcified plaque), presented in the context of vasculature pathology using the EAN obtained by a polynomial approach. Application of this material differentiation methodology using DECT has shown promising increase in contrast between materials compared to its SECT HU image counterpart.

When compared to the stoichimetric method which this study acknowledged as a standard in producing highely accurate EAN based on DECT image, polynomial approach showed to out perform in terms of calibration accuracy. Of the fitting process, 3rd degree polynomial was selected in pursuit of close adherence to the line of best fit with R^2 close to unity, while avoiding a consequential problem of overfitting from excessive level of polynomial degree used. The calibration result illustrated in Fig. 2 and 3, as discussed in the result section with detail, indicates that EAN image obtained with the polynomial approach to be more accurate than that of Stoichiometric method.

Again, Fig. 8 shows the DECT EAN image to have clearer differentiation between iodine contrast and calcium compared to its SECT HU counterpart. This goes on to show a notable utility of an EAN information in differentiating anatomical materials; Delineating and quantifying a calficified plaque in the presence of contrast in coronaty arteries is pivotal in accurate diagnosing as well as monitoring, affecting from disease prevention to treatment outcome.

The limitation of the study, thereby a direction of future investigation is as follows. First is to acknowledge wide ranges of concentrations of contrast used in clinical scenarios as well as that of calcified plaques. Collection of data and extraction of their EAN number is in order. Second is the investigation into obtaining EAN in a clinical scenario, based from an actual CT image. Through the novel polynomial method that this study proposes, further investigation and refinement of this

methodology is expected to have the potential to be applied to various imaging in quantification and delineation of materials.

5. Conclusion

In this study, the results of the polynomial approach contributed to the improvement of accuracy in calibration and extraction of information about the EAN. Since it shows superior results in enhancing the contrast between calcification and contrast agents in vessels compared to the traditional HU images, the EAN imaging based on the polynomial approach can be helpful in material quantification and separation. Therefore, it is expected to be applicable not only in vascular imaging but also in various medical image quantifications.

Acknowledgements

This paper was supported by IITP (Institute of Information & Communications Technology Planning & Evaluation). Foundation funded by the Ministry of Science and ICT (MSIT, Korea) [Project Number: 2022-0-00317]. This work was supported by the Korea Innovation Foundation (INNOPOLIS) grant funded by the Korea government (MSIT) (2023-DD-RD-0367).

References

[1] F. van Ommen, F. Kauw, E. Bennink, J. J. Heit, D. N. Wolman, J. W. Dankbaar, H. W. A. M. de Jong, and M. Wintermark, Acad. Radiol. **28**, e323 (2021).
[2] G. J. Pelgrim, R. W. van Hamersvelt, M. J. Willemink. B. T. Schmidt, T. Flohr, A. Schilham, J. Milles, M. Oudkerk, T. Leiner, and R. Vliegenthart, Eur. Radiol. **27**, 3904 (2017).
[3] D. R. Obaid, P. A. Calvert, D. Gopalan, R. A. Parker, N. E. J. West, M. Goddard, J. H. F. Rudd, and M. R. Bennett, J. Cardiovasc. Comput. Tomogr. **8**, 230 (2014).
[4] F. U. Kay, Dual-energy CT and coronary imaging, Cardiovasc. Diagn. Ther. **10**, 1090 (2020).
[5] S. Feuerlein, E. Roessl, R. Proksa, G. Martens, O. Klass, M. Jeltsch, V. Rasche, H. J. Brambs, M. H. Hoffmann, and J. P. Schlomka, Radiology **249**, 1010 (2008).
[6] J. R. Nair, C. Burrows, S. Jerome, L. Ribeiro, R. Larrazabal, R. Gupta, and E. Yu, Br. J. Radiol. **93**, 20190872 (2020).
[7] S. Nakajima, H. Ito, T. Mitsuhashi, Y. Kubo, K. Matsui, I. Tanaka, R. Fukui, H. Omori, T. Nakaoka, H. Sakura, E. Ueno, and H. Machida, Atherosclerosis **261**, 138 (2017)
[8] J. Zhu and S. N. Penfold, Med. Dosim. **43**, 2845 (2016).
[9] C. H. Chang, Y. C. Ni, and S. P. Tseng, J. Xray Sci. Technol. **29**, 317 (2021).
[10] I. Yohannes, D. Kolditz, O. Langner, and W. A. Kalender, Phys. Med. Biol. **57**, 1173 (2012).
[11] W. Schneider, T. Bortfeld, and W. Schlegel, Phys. Med. Biol. **45**, 459 (2000).